TUMOR IMMUNOLOGY

Impaired enolase 1 glycolytic activity restrains effector functions of tumor-infiltrating CD8$^+$ T cells

Lelisa F. Gemta[1], Peter J. Siska[2,3], Marin E. Nelson[4], Xia Gao[5], Xiaojing Liu[5], Jason W. Locasale[5], Hideo Yagita[6], Craig L. Slingluff Jr.[7], Kyle L. Hoehn[8], Jeffrey C. Rathmell[3], Timothy N. J. Bullock[1]*

In the context of solid tumors, there is a positive correlation between the accumulation of cytotoxic CD8$^+$ tumor-infiltrating lymphocytes (TILs) and favorable clinical outcomes. However, CD8$^+$ TILs often exhibit a state of functional exhaustion, limiting their activity, and the underlying molecular basis of this dysfunction is not fully understood. Here, we show that TILs found in human and murine CD8$^+$ melanomas are metabolically compromised with deficits in both glycolytic and oxidative metabolism. Although several studies have shown that tumors can outcompete T cells for glucose, thus limiting T cell metabolic activity, we report that a down-regulation in the activity of ENOLASE 1, a critical enzyme in the glycolytic pathway, represses glycolytic activity in CD8$^+$ TILs. Provision of pyruvate, a downstream product of ENOLASE 1, bypasses this inactivity and promotes both glycolysis and oxidative phosphorylation, resulting in improved effector function of CD8$^+$ TILs. We found high expression of both enolase 1 mRNA and protein in CD8$^+$ TILs, indicating that the enzymatic activity of ENOLASE 1 is regulated posttranslationally. These studies provide a critical insight into the biochemical basis of CD8$^+$ TIL dysfunction.

INTRODUCTION

Although the prognostic value of CD8$^+$ tumor-infiltrating lymphocytes (CD8$^+$ TILs) has been reported in various types of cancers (*1*–*3*), the progressive loss of proliferative and effector function (exhaustion) of these cells (*4*, *5*) is a major factor in diminishing antitumor immunity. The tumor microenvironment (TME) can promote TIL exhaustion via multiple cellular and molecular mechanisms, among which the expression of checkpoint inhibitory molecules, such as programmed death ligand 1 (PD-L1), has proven clinically tractable. Blocking the inhibitory signals that TILs receive promotes the activation, expansion, and effector activity of TILs (*6*, *7*). Several studies have defined nodes of transcriptional and enzymatic activity that are regulated by checkpoint molecules (*8*–*10*), but the underlying biochemical mechanism by which these inhibitors mediate the exhaustion of TILs is still poorly understood. Previous studies showed that the inhibitory checkpoint signals (*11*) and the TME (*12*–*14*) alter the metabolic activity of TILs.

There is a strong link between activation-induced proliferation and effector function of T cells and their metabolic activity (*15*–*17*). In CD8$^+$ T cells, glucose metabolism is induced initially by T cell receptor (TCR) signaling up-regulating cMYC expression (*18*, *19*) and is sustained by the mammalian target of rapamycin complex 1–hypoxia inducible factor 1 subunit α (mTORC1-HIF1α) pathway with support from cytokines in a 3-phosphoinositide–dependent protein kinase 1 (PDK1)–dependent manner (*20*, *21*). These signals promote glucose uptake and utilization (*22*–*25*). T cell activation induces both glycolytic metabolism and mitochondrial oxidative phosphorylation (OXPHOS), with a more substantial increase occurring in glycolysis (*17*, *26*). Glycolytic metabolism is essential for rapidly dividing cells such as activated T cells, which are thought to trade the adenosine 5′-triphosphate (ATP) production efficiency of OXPHOS for the faster biosynthetic precursor- and ATP-production rate of glycolysis to rapidly produce macromolecules and energy (*27*–*29*). T cells that are activated in the absence of glucose (*15*) or under conditions that prevent them from engaging glycolysis (*17*) have deficits in their effector function, indicating that glycolytic metabolism contributes to more than the production of essential building blocks. Moreover, T cells with impaired functional activity, such as anergic T cells (*30*) and exhausted T cells in chronic viral infection (*31*), are known to have attenuated glycolytic and/or oxidative metabolism. Thus, limited metabolism constrains T cell function.

Recent studies have begun to discern that TIL dysfunction is associated with disrupted glucose metabolism. Competition between tumor cells and CD8$^+$ TILs for the limited amount of glucose in the TME results in attenuated glycolytic metabolism and effector function in CD8$^+$ TILs (*11*, *13*). Further, CD8$^+$ TILs have also been reported to undergo progressive loss of mitochondrial biogenesis and function, in both murine and human settings (*12*, *32*), limiting ATP production. Enhancing the capacity of in vitro–activated T cells to produce the glycolytic intermediate, and pyruvate precursor, phosphoenolpyruvate (PEP) increases their antitumor activity after adoptive transfer into tumor-bearing mice (*13*). These studies imply that glucose deprivation prevents T cells from generating the critical glycolytic intermediates that are necessary for T cell function. However, in ex vivo studies, dysfunctional TILs retained their low metabolic and functional activities in the presence of supra-physiological levels of glucose (*11*), suggesting the existence of T cell–intrinsic restraint on glycolysis that remains to be elucidated.

To identify the intrinsic regulator in CD8$^+$ TIL glucose metabolism, here we examined the metabolic activity of CD8$^+$ TILs, quiescent CD8$^+$ T cells, and proliferative effector CD8$^+$ T cells (T_{eff}). We found that CD8$^+$ TILs exhibit a posttranslational regulation of the critical glycolytic enzyme ENOLASE 1 (also known as alpha enolase), leading to a deficit in PEP and its downstream metabolite pyruvate. Bypassing ENOLASE 1 by providing these metabolites partially restored multiple facets of the CD8$^+$ TIL metabolism and effector

[1]Department of Pathology, University of Virginia, Charlottesville, VA 22908, USA. [2]Department of Internal Medicine III, University Hospital Regensburg, 93053 Regensburg, Germany. [3]Department of Pathology, Microbiology, and Immunology, Vanderbilt University Medical Center, Nashville, TN 37232, USA. [4]Department of Pharmacology, University of Virginia, VA 22908, USA. [5]Department of Pharmacology and Cancer Biology, Duke University, NC 27710, USA. [6]Department of Immunology, Juntendo University School of Medicine, Tokyo, Japan. [7]Department of Surgery, University of Virginia Health System, Charlottesville, Virginia 22908, USA. [8]School of Biotechnology and Biomolecular Sciences, University of New South Wales, Sydney, NSW, Australia.
*Corresponding author. Email: TB5V@virginia.edu

function. We documented that a combination therapy consisting of cytotoxic T-lymphocyte associated protein 4 (CTLA-4), PD-1, and T cell immunoglobulin and mucin-domain containing-3 (TIM-3) blocking antibodies increased the presence of enolase-active $CD8^+$ TILs in the tumors. We propose that checkpoint blockade can promote the recruitment of $CD8^+$ TILs with higher metabolic activity and thus effector function.

RESULTS

Glucose metabolism by $CD8^+$ TILs is distinct from both quiescent $CD8^+$ T cells and T_{eff}

$CD8^+$ TILs that infiltrate B16cOVA melanoma tumors exhibit phenotypic and functional markers of exhaustion (fig. S1) in agreement with our previous report of the progressive loss of functional T_{eff} from the melanoma microenvironment (*33*). Given the importance of increased cellular metabolism for the proliferation and effector functions of T cells (*15*–*17*, *34*), we hypothesized that $CD8^+$ TILs are metabolically inactive. To test this, we compared the ex vivo metabolic activity of antigen-experienced $CD8^+$ TILs (days 12 to 15 after tumor implantation) and ovalbumin (OVA)–specific acute T_{eff} [5 days after vaccination with combination of OVA, anti-CD40, and polyinosinic: polycytidylic acid (poly I:C)], the latter of which were proliferative and had multiple effector activities. We used naive $CD8^+$ T cells and late [day 12/(d12)] OVA-specific T_{eff}, whose initial exposure to cognate antigen was synchronized to the time of tumor inoculation, as controls for metabolic quiescence and to control for potential age-related down-regulation of metabolic activity. A real-time metabolic assay via extracellular flux (Seahorse) analysis of FACS (fluorescence-activated cell sorting)–sorted $CD8^+$ T cell populations (sorted on the basis of CD44 expression and major histocompatibility complex–dextramer binding as described in more detail in Materials and Methods) identified that $CD8^+$ TILs had a significantly lower ECAR (extracellular acidification rate), a measure of glycolytic metabolism, than acute T_{eff} (Fig. 1A). ECAR measures media acidification as a result of the production of protons from the conversion of pyruvate (the end product of glycolysis) to lactate. These assays were performed in the presence of the physiological concentration of glucose (10 mM) reported in mouse blood and spleen (*13*) to eliminate glucose availability as a potential limitation on glycolysis. To confirm the attenuated glycolytic metabolism observed in $CD8^+$ TILs, we took advantage of radiotracer assays in which the consumption of radioactive glucose ([3-^{3}H]glucose) in glycolysis leads to the liberation of tritiated water ([^{3}H]H_2O) (*35*). $CD8^+$ TILs produced five- to sixfold less [^{3}H]H_2O than acute T_{eff} (Fig. 1B), confirming the low glycolytic activity of $CD8^+$ TILs. However, $CD8^+$ TILs were glycolytically more active than naive $CD8^+$ T cells (Fig. 1B) [which were metabolically quiescent (*16*)] and late T_{eff} (Fig. 1C).

We next investigated whether $CD8^+$ TILs have low glycolytic metabolism as a result of preferential reliance on OXPHOS. OXPHOS was determined by quantifying the amount of oxygen consumption from the media [oxygen consumption rate (OCR)]. We found that $CD8^+$ TILs had a lower OCR than acute T_{eff} (Fig. 1D) both under basal conditions and in response to an uncoupler of mitochondrial OXPHOS [fluoro-carbonyl cyanide phenylhydrazone (FCCP)] that allows the determination of maximum OCR. As with ECAR, the OCR of $CD8^+$ TILs was higher than that of the naive $CD8^+$ T cells and late T_{eff} (Fig. 1E). In agreement with the real-time metabolic analysis, an ATP-dependent luciferase assay showed that $CD8^+$ TILs had significantly higher intracellular ATP levels than naive $CD8^+$ T cells, but conversely significantly lower levels than acute T_{eff} (Fig. 1F).

$CD8^+$ TILs express glucose transporter GLUT1 and efficiently take up glucose

A potential cause of low metabolic activity in $CD8^+$ TILs could be low glucose availability in the TME (*11*, *13*). However, in the ex vivo extracellular flux assay system, we used pure $CD8^+$ TILs and the physiological level of glucose (10 times the amount reported in TMEs), which argued against competition being the sole limiting factor for $CD8^+$ TIL metabolism (*11*, *13*). An alternative possibility was that $CD8^+$ TILs failed to take up glucose owing to compromised expression of transporters. However, quantitative polymerase chain reaction (qPCR) analysis of the mRNA levels of *Glut1* [the major glucose transporter used by T cells (*36*)] and *Glut3* showed higher expression of these transcripts in $CD8^+$ TILs than in naive T cells or T_{eff} (fig. S2A). Flow cytometric analysis of glucose transporter 1 (GLUT1) protein also identified that the proportion of $CD8^+$ TILs that expressed GLUT1 protein was higher than that of naive $CD8^+$ T cells (75%) and similar to that of T_{eff} (99%, Fig. 2A). On a per-cell basis, $CD8^+$ TILs expressed the highest amount of GLUT1 [geometric mean fluorescence intensity (GMFI) = 1075] compared with naive $CD8^+$ T cells and acute T_{eff} (GMFI = 255 and 820, respectively, Fig. 2A). The expression level of GLUT1 protein on $CD8^+$ TILs was also higher than that on late T_{eff} (fig. S2B). Consistent with the high level of GLUT1 expression, we found that $CD8^+$ TILs were more effective than late T_{eff} and as effective as acute T_{eff} at taking up glucose, as quantified by the uptake of fluorescent glucose analog 2-deoxy-2-[(7-nitro-2,1,3-benzoxadiazol-4-yl)amino]-D-glucose (2-NBDG) (*37*) (Fig. 2B). Furthermore, adoptive transfer of in vitro–activated, GLUT1-overexpressing OT-1 (2×10^6 cells per mouse, activated in vitro for 3 days with anti-CD3 and anti-CD28) into B16cOVA tumor-bearing mice did not improve tumor control (Fig. 2C). Collectively, these data argued that glucose uptake was not the limiting factor that drove $CD8^+$ TIL glycolytic deficiency.

The sustained expression of GLUT1 and glycolytic machinery in CD8 T cells is promoted by contributions of signals from PDK1, mTORC1, and HIF1α (Fig. 3A) (*20*, *38*, *39*). To determine whether $CD8^+$ TILs had defects in these signaling components that could affect their glycolytic activity, we performed single-cell flow cytometric analysis of phospho-PDK1 (p-PDK1) and phospho-mTORC1 (p-mTORC1) and HIF1α. Note that PDK1 was detected using an antibody specific for the autophosphorylation site (S244) and thus reflects PDK1 expression levels rather than any differences in intrinsic activity. We found that these signaling components were activated to a similar level in $CD8^+$ TILs and acute T_{eff}. Expression of p-PDK1, p-mTORC1, and HIF1α was considerably higher in $CD8^+$ TILs than in late T_{eff}, indicating that $CD8^+$ TILs retained the ability to respond to stimuli that can promote the transport and metabolism of glucose (Fig. 3, B to D). Given the importance of mTORC1 activity in glycolysis, we further investigated its activity by measuring the levels of p-4E-BP1 and pS6, downstream targets of mTORC1. We found no substantial difference in the activity of mTORC1 between acute T_{eff} and $CD8^+$ TILs (Fig. 3E). Together, these data suggested that the glycolytic deficiency of $CD8^+$ TILs was driven by a cell-intrinsic mechanism that is downstream of glucose uptake and was independent of the canonical signaling pathways that promoted glycolysis.

$CD8^+$ TILs have low levels of PEP and enolase activity

To determine whether a defect lying within the glycolytic pathway and downstream of glucose uptake was responsible for the low metabolic activity of $CD8^+$ TILs, we performed a metabolomic analysis

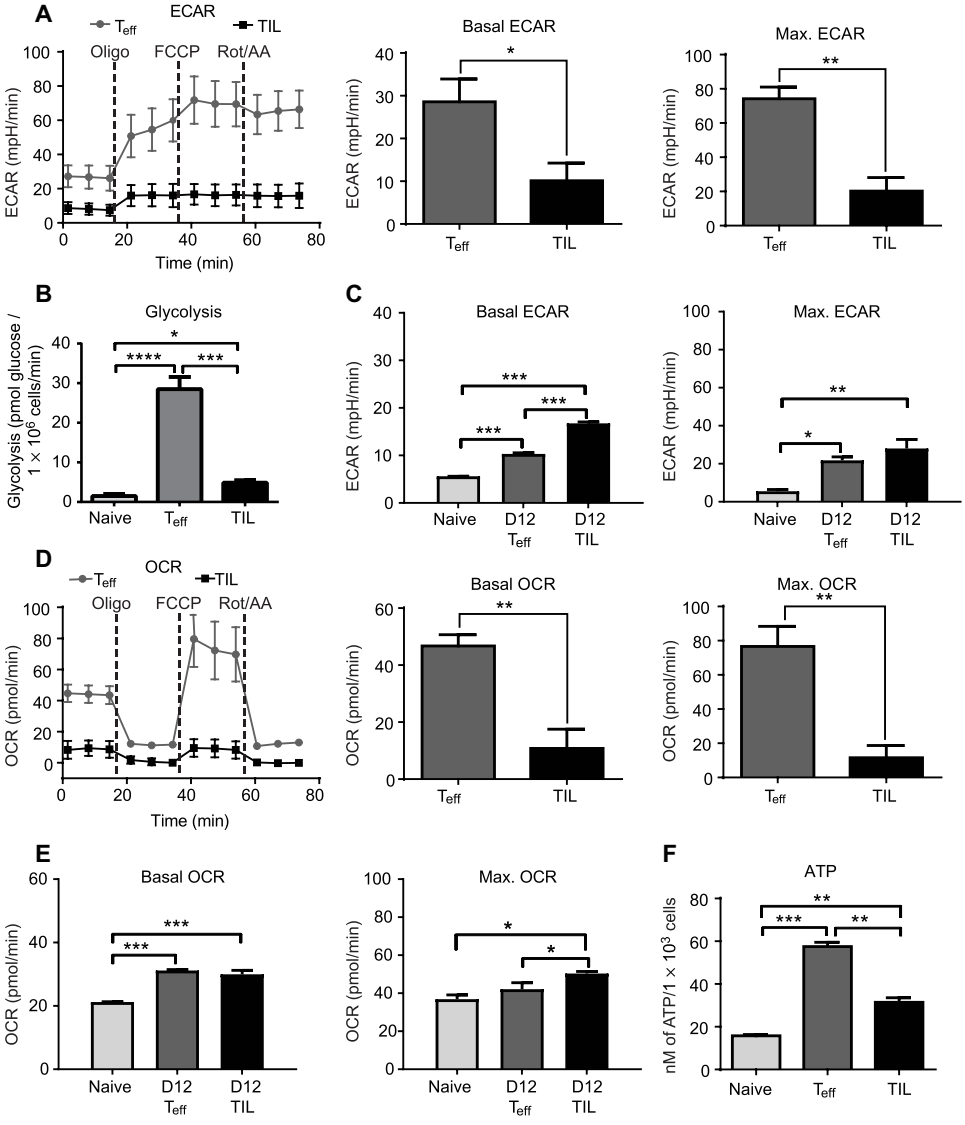

Fig. 1. CD8$^+$ TILs are metabolically less active than acute T_{eff}, but more active than quiescent CD8$^+$ T cells. (**A** to **F**) Naive and antigen-specific T_{eff} (day 5 and day 12) were FACS-sorted from the spleens of C57Bl/6 mice immunized with OVA protein, poly I:C, and anti-CD40, whereas antigen-experienced CD8$^+$ TILs were FACS-sorted from B16cOVA melanoma tumors that developed subcutaneously in C57Bl/6 mice for 12 to 15 days. (A to C) Ex vivo T cell glycolytic metabolism as measured by the ECAR (A and C) or the amount of tritiated water ([^{3}H]H_2O) released from [3-^{3}H]glucose during glycolysis (B). The basal ECAR was measured in unmanipulated cells, whereas the maximum ECAR was quantified after exposing cells to a mitochondrial ATP synthase inhibitor (1 μM oligomycin) during the extracellular flux assay. (D and E) Oxidative metabolism (OXPHOS) of the cells in (A) and (C) as quantified by OCR. Basal OCR was from sorted cells in the steady state, whereas maximum OCR was from cells in response to exposure to an uncoupler of mitochondrial OXPHOS (1 μM FCCP). (F) Intracellular ATP levels in sorted ex vivo naive CD8$^+$ T cells, day 5 (d5) T_{eff}, and d14 CD8$^+$ TILs as measured by a luciferase-based ATP determination kit. Data in (A), (C), (D), and (E) are representative of at least three independent experiments where samples were sorted from $n = 3$ to 5 mice per group and then pooled in each experiment. Data used to generate the graph in (B) were compiled from two independent experiments where the indicated sorted T cell samples were pooled from $n = 5$ to 9 mice per group. Data in (F) are representative of three independent experiments with samples pooled from $n = 3$ to 5 mice per group in each experiment. Data in (A) and (D) show means ± SEM and are analyzed by unpaired Student's t test. Data in (B), (C), (E), and (F) show means ± SEM and analyzed by one-way ANOVA, followed by Tukey's multiple comparison test. *$P < 0.05$, **$P < 0.01$, ***$P < 0.001$, ****$P < 0.0001$.

[an unbiased assessment of the relative cellular metabolite composition (*40*)]. We identified a significant (~10-fold) reduction in the steady-state level of PEP in CD8$^+$ TILs compared with acute T_{eff} (Fig. 4A). The relative abundance of the glycolytic metabolites upstream of PEP was similar (Fig. 4A and fig. S3A), implying that the PEP production step of glycolysis is the point at which glycolysis is disrupted in CD8$^+$ TILs. Furthermore, low levels of pyruvate were found in CD8$^+$ TILs, arguing that excessive PEP-to-pyruvate conversion did not account for the low levels of PEP (Fig. 4A). Therefore, we hypothesized that PEP deficiency in CD8$^+$ TILs was mediated by reduced expression or activity of ENOLASE 1, the enzyme that is responsible for PEP production in glycolysis. Unexpectedly, qPCR and Western blot analysis of enolase 1 in FACS-purified CD8$^+$ T cell populations demonstrated that the mRNA and protein levels of *eno1*/ENOLASE 1 were similar between acute T_{eff} and CD8$^+$ TILs (Fig. 4B). Intracellular flow cytometric analysis confirmed that equivalent proportions of T_{eff} and TILs express ENOLASE 1 and that the level of ENOLASE 1 expression in acute T_{eff} and CD8$^+$ TILs was similar (Fig. 4C). We also found that the mRNA levels of many glycolytic enzymes were equivalent between acute T_{eff} and CD8$^+$ TILs (fig. S3, B and D). However, significantly higher amounts of the mRNAs of glycolytic enzymes were observed in CD8$^+$ TILs than in age-matched d14 T_{eff} (fig. S3, C and D), confirming the notion that CD8$^+$ TILs were not metabolically quiescent as shown previously in Fig. 1 (C and E). Together, these data demonstrated that the glycolytic metabolism of CD8$^+$ TILs was altered at the level of PEP production by factors other than the availability of the precursor metabolites or the enzymes responsible for production of PEP.

To understand whether the ENOLASE 1 protein in CD8$^+$ TILs had compromised enzymatic activity that could result in PEP deficiency, we directly assessed enolase activity in lysates prepared from FACS-sorted CD8$^+$ T cell populations. We found a notable deficit in enolase activity in CD8$^+$ TILs compared with acute T_{eff} (Fig. 4E, left). Furthermore, enolase activity did not increase in FACS-sorted CD8$^+$ TILs after a strong in vitro T cell stimulation achieved by cross-linking TCR with anti-CD3 in the presence of anti-CD28. In contrast, in vitro T cell stimulation resulted in a marked up-regulation of the enolase activity in FACS-sorted acute T_{eff}, assessed in parallel (Fig. 4E, right). Together, these data supported the hypothesis that CD8$^+$ TIL glycolytic metabolism was restrained by enolase activity rather than by

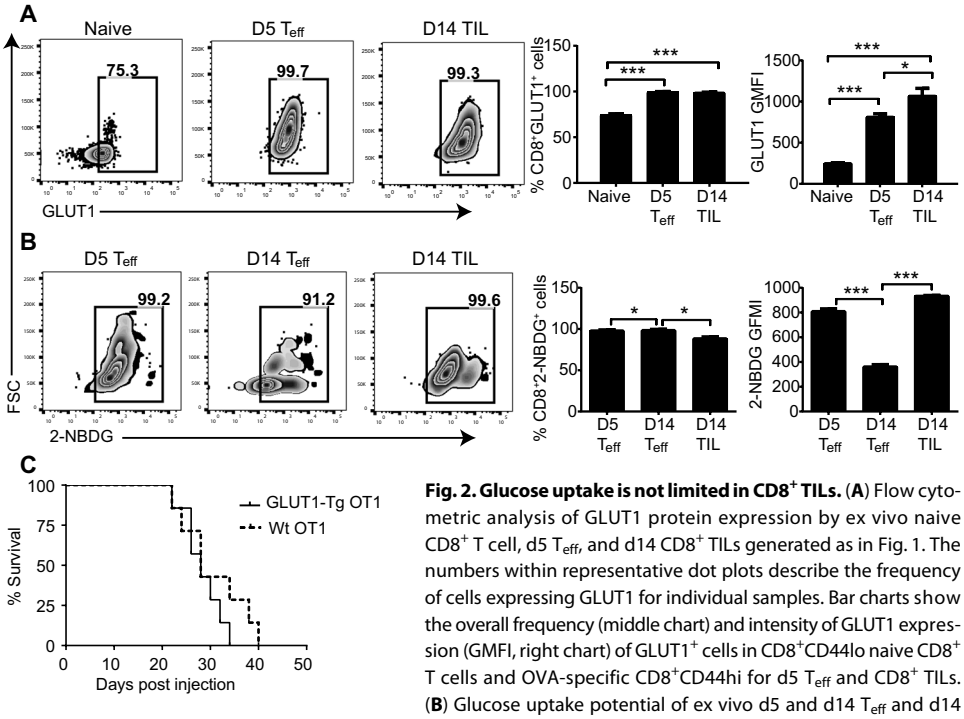

Fig. 2. Glucose uptake is not limited in CD8$^+$ TILs. (**A**) Flow cytometric analysis of GLUT1 protein expression by ex vivo naive CD8$^+$ T cell, d5 T_{eff}, and d14 CD8$^+$ TILs generated as in Fig. 1. The numbers within representative dot plots describe the frequency of cells expressing GLUT1 for individual samples. Bar charts show the overall frequency (middle chart) and intensity of GLUT1 expression (GMFI, right chart) of GLUT1$^+$ cells in CD8$^+$CD44lo naive CD8$^+$ T cells and OVA-specific CD8$^+$CD44hi for d5 T_{eff} and CD8$^+$ TILs. (**B**) Glucose uptake potential of ex vivo d5 and d14 T_{eff} and d14 CD8$^+$ TILs as measured by flow cytometry after pulsing cells with the fluorescent glucose analog 2-NBDG. The frequency (middle chart) of 2-NBDG$^+$ cells and amount of uptake (right chart) within the OVA-specific CD8$^+$CD44hi cell population are shown. (**C**) Survival of B16cOVA tumor-bearing mice was assessed after adoptive transfer of in vitro–activated nontransgenic or GLUT1 transgenic OT-1 T cells 5 days after subcutaneous tumor injection. Data in (A) and (B) are representative of three to five independent experiments, with at least two mice per group in each experiment. Data in (C) are from $n = 7$ mice per group, and the experiment was repeated twice. Data show means ± SEM: one-way ANOVA, followed by Tukey's multiple comparison test. *$P < 0.05$, ***$P < 0.001$.

enolase expression, implying that enolase function was regulated at the posttranslational level in CD8$^+$ TILs.

Overcoming PEP deficiency rescues metabolic and functional activity of CD8$^+$ TILs

During glycolysis, PEP serves as a substrate for synthesis of pyruvate, which can promote glycolysis via generation of nicotinamide adenine dinucleotide (NAD^+) in a metabolic program known as aerobic glycolysis (the Warburg effect) and also fuels OXPHOS through the mitochondrial tricarboxylic acid cycle (*28*). Given the low glycolytic and OXPHOS metabolism, despite the high glucose uptake that we observed in CD8$^+$ TILs, we speculated that providing exogenous pyruvate (bypassing glycolysis or, more specifically, overcoming the PEP shortage) should rescue CD8$^+$ TIL aerobic glycolysis and OXPHOS. Exogenous pyruvate provided during metabolic flux analysis of FACS-sorted, ex vivo CD8$^+$ TILs significantly increased the CD8$^+$ TIL basal ECAR, yet had no impact on acute T_{eff} basal ECAR (Fig. 5, A and B, Basal ECAR). The lack of effect of exogenous pyruvate on acute T_{eff} presumably occurred because these cells produced sufficient pyruvate. Provision of pyruvate also substantially increased the maximal ECAR achieved by CD8$^+$ TILs (measurement of ECAR in the presence of oligomycin, which inhibits OXPHOS and forces cells to be dependent on glycolysis for ATP production, Fig. 5, A and B, Max. ECAR). Exogenous pyruvate also enhanced both the basal and maximal OXPHOS in CD8$^+$ TILs and acute CD8$^+$ T_{eff} (Fig. 5, A and B, Basal OCR and Max. OCR), suggesting that glycolytic or pyruvate deficiency could be limiting the OXPHOS capability of CD8$^+$ TILs. During a 4-hour in vitro stimulation, the addition of pyruvate resulted in a significant increase in the frequency of CD8$^+$ TILs that produced interferon-γ (IFN-γ) and tumor necrosis factor–α (TNFα) (Fig. 5C). Similar results were observed when we provided exogenous PEP to the CD8$^+$ TILs during the short-term in vitro cultures (Fig. 5D), suggesting that PEP shortage impairs CD8$^+$ TIL function by limiting pyruvate availability. Together, these data indicated that low enolase activity impaired the metabolic activity and contributed to the lowered functional activity observed in CD8$^+$ TILs.

To further interrogate the contribution of enolase activity to CD8$^+$ T cell function, we investigated cytokine production after treating T_{eff} and CD8$^+$ TILs with sodium fluoride (NaF), a well-studied enolase inhibitor (*41*, *42*). Consistent with the reported inhibitor effect of NaF on enolase activity in other cell types, NaF strongly inhibited enolase activity in T_{eff} when added to cell culture during acute in vitro stimulation (fig. S4A, cells). Furthermore, NaF completely inhibited enolase activity (fig. S4A, lysate) when added to the lysates of untreated T_{eff} 5 min before assay, suggesting that the reduction in enolase activity as a result of the NaF treatment of cell culture was due to the direct effect of NaF on enolase. NaF substantially reduced cytokine production from T_{eff} after in vitro culture with peptide-pulsed antigen-presenting cells (fig. S4, B and C), further supporting the importance of enolase activity to the effector function of T cells. NaF also significantly reduced the remaining cytokine production from CD8$^+$ TILs (fig. S4, B and C, and Fig. 5C), indicating that although it was relatively weak, the activity of enolase in CD8$^+$ TILs played an important role in supporting the residual effector function observed in these cells. Together, these results indicated that deficiency in enolase activity limited the effector function of CD8$^+$ TILs.

Immune checkpoint blockade therapy recruits enolase-active CD8$^+$ TILs into tumors

PD-1 has been reported to inhibit glycolytic metabolism in human CD4$^+$ T cells (*43*). Consistent with this, a recent study has shown that blockade of either PD-1 or CTLA-4 augments the glycolytic metabolism in CD8$^+$ TILs responding to mouse sarcoma tumors (*11*). This led us to ask whether immune checkpoint signals constrained enolase activity in CD8$^+$ TILs. We treated mice bearing tumors established for 9 days with a combination of checkpoint blocking antibodies (anti–PD-1, anti–CTLA-4, and anti–TIM-3 every 3 days). This treatment regimen increased the absolute number of CD8$^+$ TILs in the tumors (Fig. 6A) and constrained tumor outgrowth (Fig. 6B) compared with controls. This combinatorial checkpoint molecule inhibition (CPi) did not have a significant

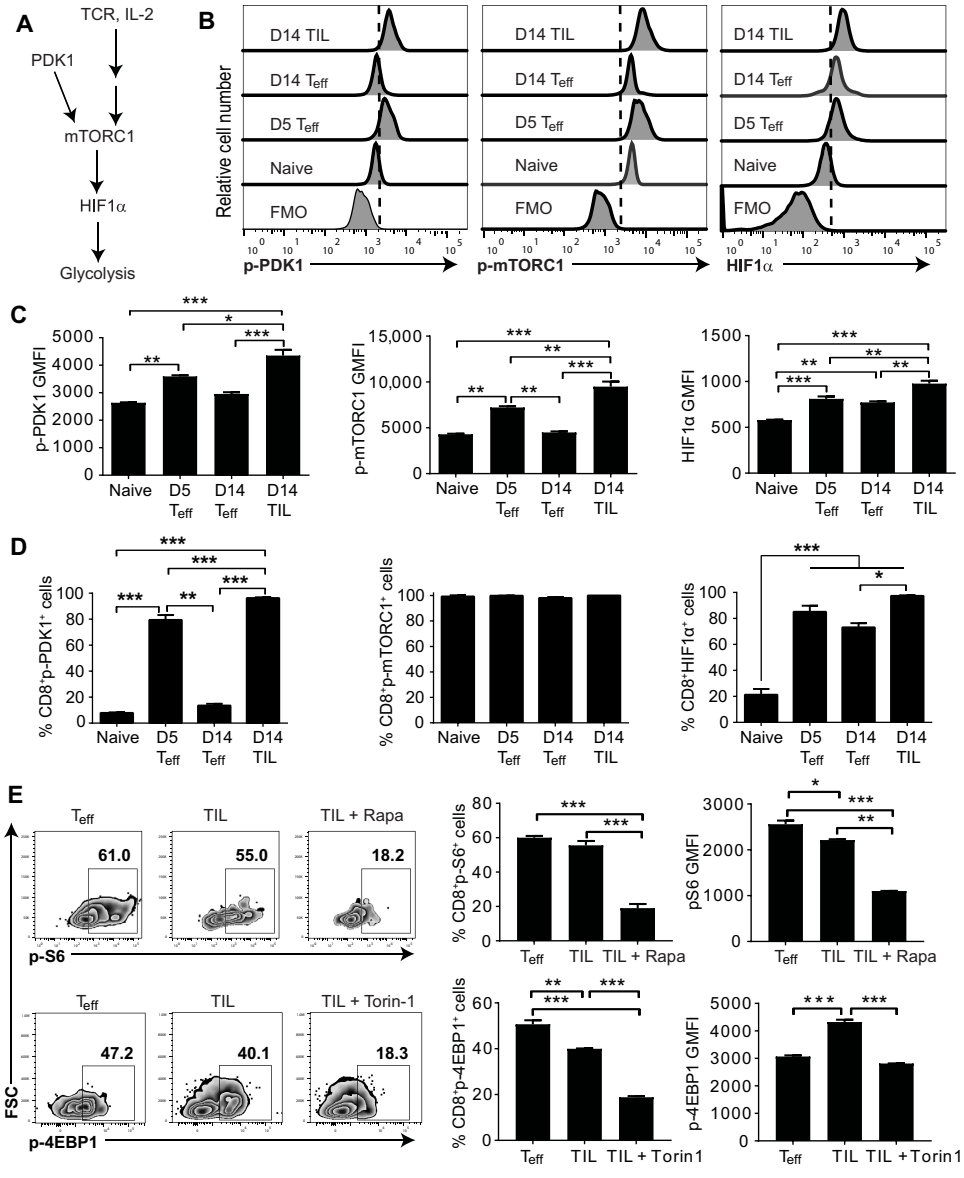

Fig. 3. Glycolysis-regulating signaling molecules are expressed and active in CD8$^+$ TILs. (**A**) The signaling pathway downstream of TCR and cytokine signals that are known to promote the glucose uptake and glycolysis. (**B** to **D**) Flow cytometric analysis of p-PDK1 (Ser^{244}), p-mTORC1 (Ser^{2448}), and HIF1α expression in naive CD8$^+$ T cells and OVA-specific d5 T_{eff}, d14 T_{eff}, and d14 CD8$^+$ TILs that were prepared as in Fig. 1. (C) GMFI of pPDK1, p-mTORC1, and HIF1α in the CD8$^+$CD44lo naive or OVA-specific CD8$^+$CD44hi T_{eff} and TILs expressing the protein of interest. (D) The frequency of p-PDK1$^+$, p-mTORC1$^+$, or HIF1α$^+$ cells within naive CD8$^+$CD44lo and OVA-specific CD8$^+$CD44hi T_{eff} and TILs. (**E**) Phosphoflow cytometric analysis of mTORC1 activity via determination of the phosphorylated downstream targets (S6 and 4E-BP1) after 1-hour in vitro stimulation of acute T_{eff} and CD8$^+$ TILs with anti-CD3 (5 μg/ml). The CD8$^+$ TIL in vitro stimulation was also conducted in the presence of 250 μM rapamycin to inhibit pS6 or 250 μM Torin-1 to inhibit p4E-BP1 for staining negative control. Data in (B) to (D) are representative of three to five independent experiments, with at least two mice per group in each experiment. Data in (E) are from samples pooled from $n = 5$ to 6 mice per group, and the experiment was repeated twice. Data show means ± SEM: one-way ANOVA, followed by Tukey's multiple comparison test. *$P < 0.05$, **$P < 0.01$, ***$P < 0.001$.

effect on the expression of ENOLASE 1 (Fig. 6, C and D). However, the CPi treatment significantly improved enolase activity in CD8$^+$ TILs (Fig. 6E). To determine the relative contribution of the inhibition of PD-1, CTLA-4, or TIM-3 to the increased enolase activity, we treated tumor-bearing mice with antibodies targeting individual checkpoint molecules. Checkpoint monotherapies did not significantly improve enolase activity in CD8$^+$ TILs (Fig. 6F). Together, these results indicated that multiple checkpoint signals contributed to the low enolase activity observed in CD8$^+$ TILs.

To understand the contribution of enolase activity to the antitumor effects of the CPi-treated CD8$^+$ TILs, we investigated the impact of inhibiting enolase on the cytokines and lytic molecules (e.g., perforin) production by the CPi-treated CD8$^+$ TILs. Treatment of CPi-treated CD8$^+$ TILs with NaF significantly reduced the capacity of the CPi-treated CD8$^+$ TILs to produce IFN-γ and perforin (fig. S5, A and B). These data suggested that the increase in enolase activity in the CPi-treated CD8$^+$ TILs contributed to the antitumor activity of these cells.

We next investigated whether the CPi treatment increased enolase activity in CD8$^+$ TILs via reactivation of enolase in pre-existing intratumoral CD8$^+$ TILs or by inducing/sustaining enolase activity in newly infiltrating CD8 TILs. For this study, the CPi experiment was conducted in the presence or absence of a well-known S1PR-agonist, FTY-720, that blocks T cells from exiting the secondary lymphoid tissues. FTY-720 treatment abrogated the ability of CPi treatment to increase enolase activity in CD8$^+$ TILs (Fig. 6G). These data indicated that the combinatorial checkpoint molecule blockade either enhanced enolase activity in the recently activated CD8$^+$ TILs or sustained it in the newly tumor-infiltrating T cells, rather than re-activating enolase in the CD8$^+$ TILs that are already in the tumors.

CD8$^+$ TILs isolated from human melanomas have low enolase activity

To understand whether enolase activity is altered in CD8$^+$ TILs that infiltrate the human cancers, we sorted antigen-experienced (CD45RO$^+$) CD8$^+$ TILs from metastatic melanoma samples. Compared with peripheral blood mononuclear cells (PBMCs) from healthy donors that were stimulated in vitro to generate T_{eff}, human CD8$^+$ TILs produced a limited amount of IFN-γ after cross-linking the TCR (fig. S6A). Activation of human healthy donor PBMCs also strongly induced (fourfold) enolase activity as judged by direct analysis of enolase within cell lysates (fig. S6B). More than 80% of

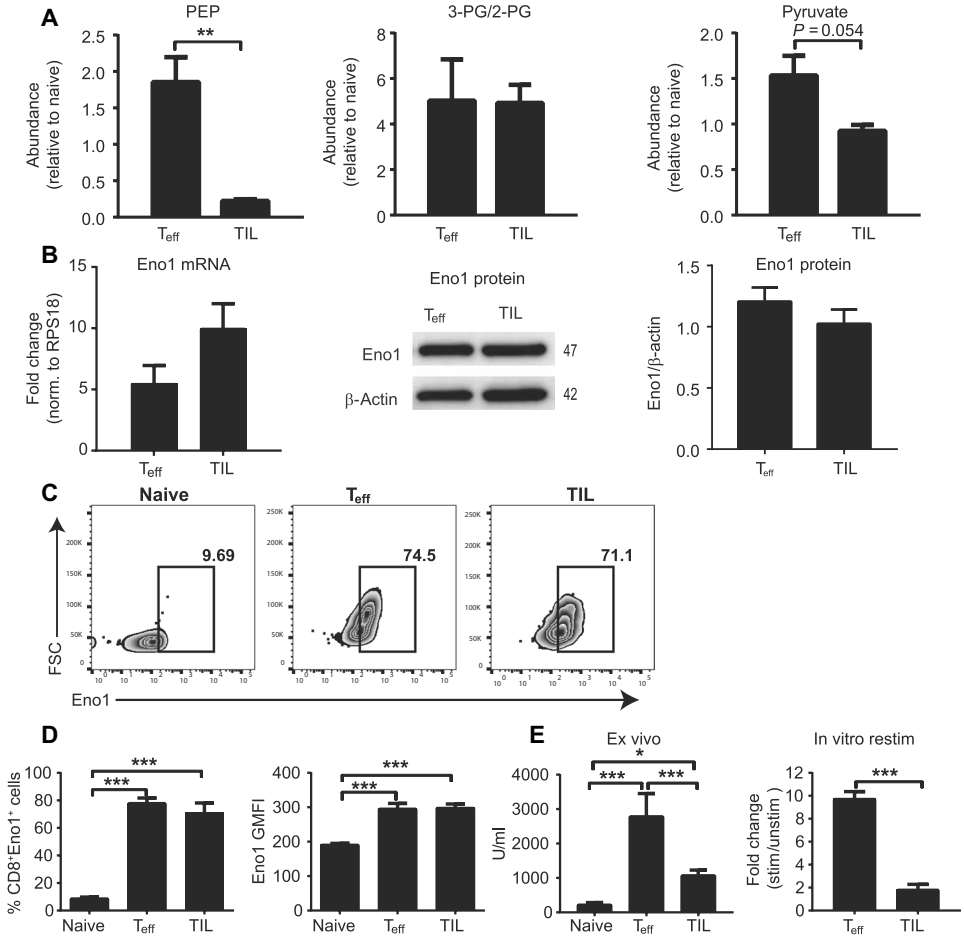

Fig. 4. Weak enolase activity restrains glucose metabolism in glycolysis in CD8$^+$ TILs. (**A**) Metabolomic analysis of the relative metabolite composition of d5 T_{eff} and d14 CD8$^+$ TILs normalized to that of naive CD8$^+$ T cells. Metabolites were extracted from similar samples to that described in Fig. 1 and subjected to mass spectrometric analysis. 3-PG/2-PG, 3-phosphoglycerate and 2-phosphoglycerate. (**B**) The expression of *enolase 1* transcripts in d5 T_{eff} and d14 CD8$^+$ TILs was measured by qPCR and ENOLASE1 protein was measured by Western blot (numbers indicate molecular weight). (**C** and **D**) Flow cytometric analysis of ENOLASE 1 protein expression in naive CD8 T cells, d5 T_{eff}, and d14 CD8$^+$ TILs. The frequencies of cells that express ENOLASE 1 within naive CD8$^+$CD44lo and OVA-specific CD8$^+$CD44hi T_{eff} or CD8$^+$ TILs are indicated. GMFI is derived from ENOLASE 1–expressing cells. (**E**) Fluorescence-based spectrophotometric analysis of enolase activity (PEP formation) measured in lysates prepared from FACS-sorted naive CD8$^+$ T cells, acute T_{eff}, and CD8$^+$ TILs either directly ex vivo (left) or after in vitro stimulation with anti-CD3 and anti-CD28 for 4 days (right). Data are on samples pooled from $n = 5$ to 9 mice per group (A), representative from two independent experiments with samples pooled from at least six mice per group (B), and are representative of three independent experiments with at least three mice per group (C and D). Data in (E) are combined from multiple independent experiments with T cells pooled from 2 to 3 mice per group. Data show means ± SEM and are analyzed by unpaired Student's *t* test (A, B, and E, right) or one-way ANOVA, followed by Tukey's multiple comparison test (D and E, left). *$P < 0.05$, **$P < 0.01$, ***$P < 0.001$.

human melanoma CD8$^+$ TILs have similar low enolase activity as observed in murine models and that their metabolic activity is likely to be similarly impeded, contributing to the observed defect in effector function.

DISCUSSION

Elevation of metabolic activity is essential for T_{eff} to support their proliferation and function (*19*, *22*, *31*). Our data support the developing notion that an underlying basis of TIL dysfunction is insufficient glycolysis and OXPHOS to support strong effector functions (*11*–*14*). This state persists even though CD8$^+$ TILs are capable of efficiently transporting glucose and have active signaling pathways that normally promote the expression of the enzymes that are involved in glucose metabolism. This indicates that CD8$^+$ TILs represent a population of cells that are undergoing constant stimulation and that their attenuated metabolic activity is not a function of immunological quiescence. Rather, glucose metabolism is constrained in CD8$^+$ TILs by weak enolase activity, which resulted in limited production of PEP, a vital glycolytic intermediate, and provision of pyruvate or PEP is sufficient to restore some of the metabolic and functional activity of CD8$^+$ TILs. The reduction in enolase activity is regulated posttranslationally. Our data show that a CPi protocol that slowed tumor outgrowth results in the infiltration of tumor by CD8$^+$ TILs with improved enolase activity. The low proliferative and functional activity of CD8$^+$ TILs, allied with their limited metabolic activity, could indicate that these cells are simply quiescent. However, compared with naive and late (age-matched) effectors, we found high levels of expression and activation of the PDK1-mTORC1-HIF1α signaling pathway, which lies downstream of the TCR and cytokine receptors. The level of activation of this pathway was equal to, or higher than, that seen in acute T_{eff}. Consistent with this, we found no defect in the expression of GLUT1, the major transporter of glucose in lymphocytes, or the ability of CD8$^+$ TILs to acquire glucose from their surroundings. Thus, the inability of CD8$^+$ TILs to consume glucose despite the expression of the glycolytic machinery indicates that the glycolytic inactivity of CD8$^+$ TILs is regulated by a functional defect in the glycolytic pathway rather than quiescence or a lack of stimulation. Although the biomarkers (i.e., signaling molecules and molecular components of glycolysis) of T cell glycolysis

the antigen-experienced human CD8$^+$ TILs (Fig. 6H) and about 50% of the antigen-experienced CD4$^+$ TILs expressed ENOLASE 1 (fig. S6D). However, consistent with our murine studies, we found limited enolase activity in both antigen-experienced CD8$^+$ TILs and CD4$^+$ TILs compared with the acutely activated human healthy donor T cells (Fig. 6I and fig. S6E). There was a trend toward higher enolase activity in 41BB (CD137)–positive compared with 41BB-negative CD8$^+$ TILs (fig. S6C), where 41BB expression identified T cells that may have recently responded to TCR stimulation (*44*). This suggested that functional enolase may correlate with T cells that maintain functional responsiveness. Thus, we conclude that

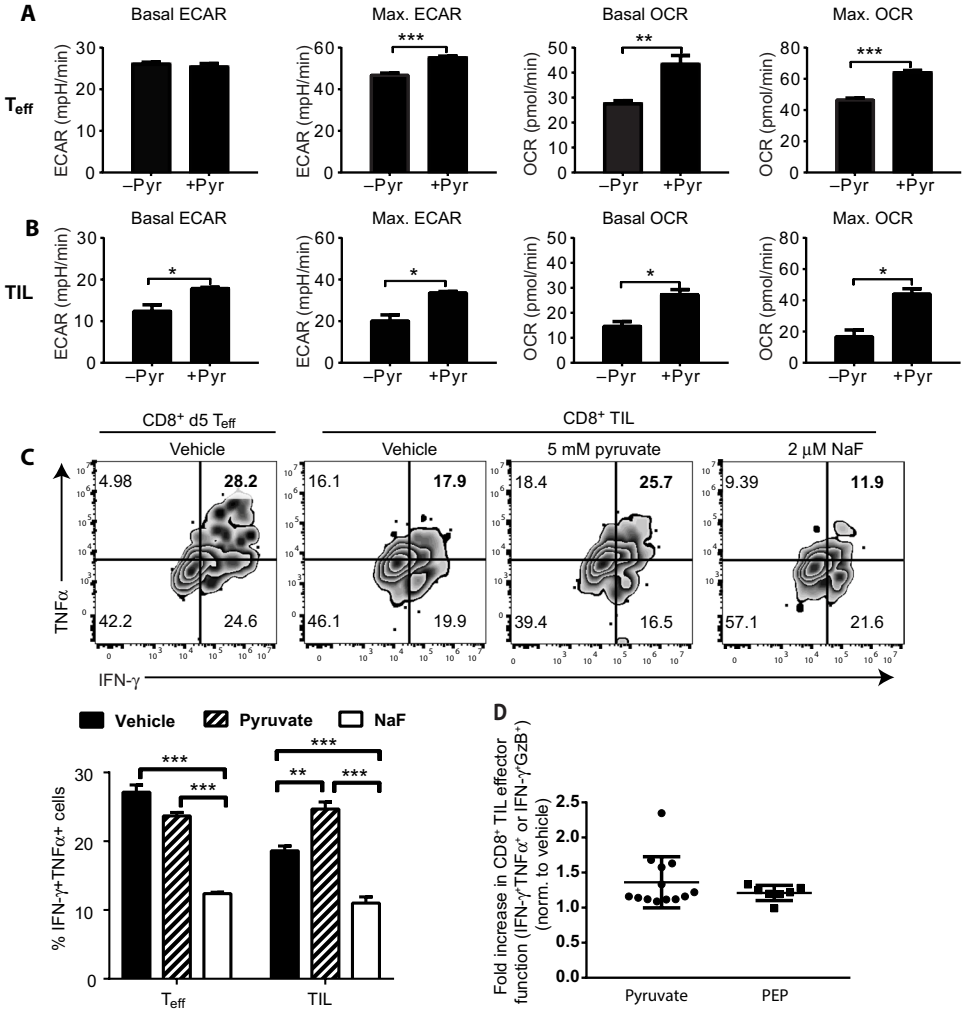

Fig. 5. Bypassing enolase restores metabolic function and effector activity in CD8$^+$ TILs. (**A** and **B**) ECAR and OCR by FACS-sorted d5 T_{eff} and d12 CD8$^+$ TILs as measured by Seahorse in pyruvate-free or 2 mM pyruvate-containing XF minimal media. Basal ECAR and basal OCR were measured without any manipulation, whereas maximum ECAR and maximum OCR were determined after oligomycin or FCCP exposure, respectively. (**C** and **D**) Intracellular flow cytometric analysis of IFN-γ and TNFα production from T_{eff} and CD8$^+$ TILs treated for 4 hours with vehicle, 5 mM pyruvate, or 2 μM NaF during in vitro culture and stimulation with OVA_{257}-pulsed antigen-presenting cells. (D) Fold increase in the proportion of CD8$^+$ T cells expressing cytokines after culturing with 5 mM pyruvate or PEP (1 μg/ml; after partial permeabilization) for 4 hours. Data are representative of two to three independent experiments and show means ± SEM. Statistical analyses were done by unpaired Student's *t* test (A, B, and D) and two-way ANOVA, followed by Tukey's multiple comparison test (C). *P < 0.05, **P < 0.01, ***P < 0.001.

correlate well with the actual metabolic activity (as judged by flux assays) of naive CD8$^+$ T cells and T_{eff}, it is important to note that there is no strong correlation between the activation state of these molecules and the overall metabolic activity of CD8$^+$ TILs; thus, the sole use of glycolytic biomarkers may overestimate the metabolic activity of CD8$^+$ TILs. This study pinpointed the mechanism responsible for restraining CD8$^+$ TIL glycolytic metabolism to weak enolase activity, which resulted in reduced levels of PEP and pyruvate. PEP can support T cell function in two major ways: by promoting cytokine production via calcium signaling (*13*) and by serving a substrate for pyruvate synthesis (*28*). A recent study has demonstrated that the antitumor activity of in vitro–activated T cells after adoptive transfer into tumor-bearing mice improves when PEP production is augmented (*13*). Our findings not only support that report but also directly show that endogenous CD8$^+$ TILs have low levels of PEP and that the shortage of this metabolite constrains both the glycolytic and mitochondrial metabolism in CD8$^+$ TILs. Unexpectedly, we did not observe accumulation of glycolytic metabolites upstream of PEP as one might expect from the loss of enolase activity. However, this is not uncommon in complicated biological systems such as glycolysis, which involves bidirectional reactions, feedback inhibition, and metabolites with multiple possible fates (*27*, *28*). For example, 2-PG (2-phosphoglycerate, enolase's substrate) can be converted back to upstream metabolite 3-PG (*45*), which can be taken out of glycolysis and be used for nucleotide and lipid synthesis via serine biosynthesis (*28*, *46*).

Our studies have found no deficiency in ENOLASE protein expression, indicating that posttranslational regulation likely impedes enolase enzymatic activity. There are several potential mechanisms of regulation of enolase activity in CD8$^+$ TILs. First, posttranslational modifications of ENOLASE 1 have been described, including phosphorylation, acetylation, and methylation (*47*), although it is unclear whether these modifications influence enolase enzymatic activity. Second, enolase enzymatic activity requires divalent cations and is inhibited by fluoride (*48*) and thus may be susceptible to ion availability in the TME. Third, in addition to enolase 1's typical cytoplasmic localization where it performs its enzymatic role, ENOLASE 1 can also be directed to the cell surface where it serves as a receptor for plasminogen (*47*), is recruited to mitochondria where it preserves mitochondrial integrity and membrane potential (*49*), or is expressed as an alternative translational product (Myc binding protein-1) that is translocated to the nucleus (*50*). Thus, the inactivity of enolase in CD8$^+$ TILs may either be a result of regulation of its enzymatic activity or repurposing of ENOLASE 1 away from glycolysis. The precise regulatory mechanism that leads to enolase in activity in TILs remains to be determined. We also do not understand whether the low enolase activity in CD8$^+$ TILs is a function of weak priming or loss within the tumor. We found that concomitant blocking of multiple immune checkpoint molecules increased the presence of CD8$^+$ TILs with more active enolase and led to a decrease in tumor outgrowth. The increase in enolase-active CD8$^+$ TILs that occurs with CPi was determined to arise from newly infiltrating T cells.

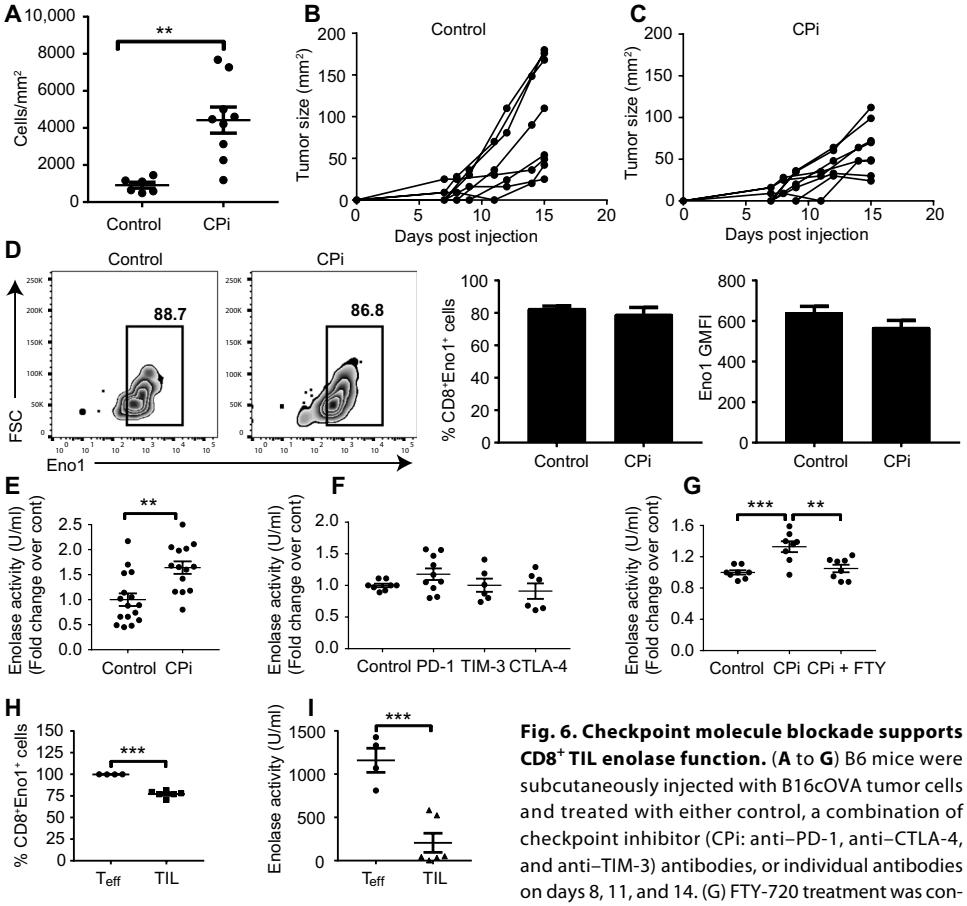

Fig. 6. Checkpoint molecule blockade supports CD8⁺ TIL enolase function. (**A** to **G**) B6 mice were subcutaneously injected with B16cOVA tumor cells and treated with either control, a combination of checkpoint inhibitor (CPi: anti–PD-1, anti–CTLA-4, and anti–TIM-3) antibodies, or individual antibodies on days 8, 11, and 14. (G) FTY-720 treatment was continuously provided through the drinking water starting on day 8 after tumor injection. All tumors were harvested on day 15 after injection. (A) The absolute numbers of antigen-experienced CD8⁺ TILs per square millimeter of tumor. (B) Tumor growth over time. (D) The frequency (left and middle) and intensity of expression (right) of enolase within OVA-specific CD8⁺CD44hi populations from control or combined CPi-treated mice. (E to G) Fluorescence-based spectrophotometric direct enolase activity (PEP formation) measurement in the lysates prepared from FACS-sorted antigen-experienced CD8⁺ TILs from control, combined-CPi (E and G), or individual-CPi–treated (F) mice in the absence (E and F) or presence of FTY-720 (G). The enolase activity in (E) and (F) was normalized to the average of the control replicates for CD8⁺ TILs to allow cross-experiment comparison. (H and I) Analysis of ENOLASE 1 expression and activity in ex vivo human CD8⁺ TILs using human healthy donor PBMCs that were in vitro stimulated with anti-CD3 and anti-CD28 for 3 days as a positive control. (**H**) Frequency of ENOLASE 1–positive cells within CD8⁺CD45RO⁺ human T_{eff} and TILs. (**I**) Fluorescence-based spectrophotometric analysis of the activity of enolase in lysates prepared from FACS-sorted CD8⁺CD45RO⁺ human T_{eff} and TILs. Data are representative of three independent experiments (A to D), combined from three to five independent experiments with samples pooled from at least three mice per group (E and F), combined from two independent experiments with at least three mice per group (G), or from two healthy donor PBMCs and three melanoma patient TILs (H and I). Data show means ± SEM and are analyzed by unpaired Student's *t* test. $^{**}P < 0.01$, $^{***}P < 0.001$.

at the periphery of the tumor, or within the circulation are also metabolically compromised.

Our current study identifies augmentation of enolase activity as an avenue for increasing TIL function, although it should be noted that the therapies targeting the combination of checkpoint molecules used in this study have yet to be evaluated clinically. We have concluded that the limited glycolysis and enolase activity exhibited by CD8⁺ TILs contributes to the remaining effector function of these cells as NaF eliminated remaining activity. Although NaF is a well-characterized inhibitor of enolase, we acknowledge that it could have other, enolase-independent impacts on T cells. Further, blocking checkpoint signals or isolating CD8⁺ TILs from the tumors (as done in the in vitro studies) did not fully restore enolase activity, suggesting the existence of additional as yet unidentified pathways regulating enolase and glycolysis. Although PEP and pyruvate were found to enhance TIL function in vitro here and in our previous studies on renal cell carcinoma (*32*), bypassing enolase inactivity in vivo with PEP or pyruvate may be challenging because PEP does not cross the cell membrane and pyruvate may be used by tumors. The most likely immediate clinical utility of pyruvate rescue approach will be to support the metabolic activity of TILs or PBMCs that are intended to be used in adoptive cell transfer protocols. These limitations in PEP- and pyruvate-based rescue approaches highlight the need to understand how enolase activity is impaired in CD8⁺ TILs.

Recent studies by others (*12*) and the data presented here show a low level of OXPHOS in CD8⁺ TILs. Although this could be attributed to low mitochondrial mass or mitochondrial membrane potential (*12*), the ability of pyruvate to rescue the OXPHOS in CD8⁺ TILs raises intriguing questions about the contribution of pyruvate deficiency to the loss of mitochondrial function. ENOLASE 1 has been previously reported to bind the mitochondrial membrane and prevent loss of membrane potential, which is essential for the OXPHOS (*49*). Whether mitochondrial binding of ENOLASE 1 supports mitochondrial function by bringing together pyruvate synthesis and mitochondria is an intriguing question that will need to be addressed. In conclusion, restoration of ENOLASE 1 activity might be expected to not only promote glycolysis but also improve the OXPHOS capabilities of TILs,

We interpret these data to mean that CPi either promotes enolase activity during CD8⁺ T cell priming or preserves enolase activity in the newly infiltrating CD8⁺ T cells as they enter the tumor. Currently, there is no assay with sufficient sensitivity to assess the enolase or glycolytic activity of CD8⁺ TILs in the early stages of their response to tumors in the draining lymph node. Sensitive metabolic assays are also required to investigate whether the weak enolase activity observed in the murine and human TILs is only apparent in those cells embedded within the tumor, or whether tumor-specific or bystander T cells within the stroma,

together substantially improving effector activity and durability within tumors.

MATERIALS AND METHODS

Study design

The objectives of the study were to determine whether the dysfunction of murine and human melanoma $CD8^+$ TILs is a function of cell-intrinsic defects in glycolytic metabolism that results in curtailed effector functions and to identify the mechanism that may attenuate the glycolytic metabolism, which could be targeted or used as a biomarker for translational purposes. For murine studies, C57BL/6 mice were either injected with B16cOVA melanoma cells or immunized with OVA protein, poly I:C, and anti-CD40. Cohort sizes were determined by power studies defined using prior tumor outgrowth kinetics. Tumors were allowed to develop for 2 to 3 weeks or until they reached the maximum size (for tumor growth studies) permitted by the protocol of the Animal Care and Use Committee of the University of Virginia (UVA). Tumor size was measured in an unblinded manner. $CD8^+$ TILs were isolated from the tumors, whereas naive $CD8^+$ T cells and antigen-specific T_{eff} were harvested from the spleens of the immunized, non–tumor-bearing mice. All the metabolic studies were done on ex vivo, FACS-sorted T cells to remove competition for nutrients with tumor cells and also the impact of tumor and other cells on the $CD8^+$ T cells. For checkpoint blockade studies, tumor-bearing mice received three doses of control immunoglobulin G (IgG) or a combination of anti–PD-1, anti–CTLA-4, and anti–TIM-3 every 3 days starting on day 8 after tumor implantation. Tumors were harvested 1 day after the last treatment for analysis. In the studies involving human samples, antigen-experienced $CD8^+$ and $CD4^+$ T cells were isolated from the tumors of patients with melanoma and PBMCs of healthy participants obtained under informed consent in compliance with UVA Human Subjects Institutional Review Board (IRB) number 10598. All animal studies were done in accordance with the UVA Animal Care and Use Committee protocol number 3292.

Tumor cell line, mice, and tumor injection

The OVA-expressing B16 melanoma cell line (B16cOVA) was previously generated in our laboratory (*51*) and was maintained in RPMI 1640 (Thermo Fisher Scientific) supplemented with 5% fetal bovine serum (FBS; Gemini Bio) in the presence of selection agent (blastocidin, Invitrogen). B16cOVA melanoma cells (4×10^5) in 100 μl of Hanks' balanced salt solution were injected subcutaneously into the shoulders or flank of male C57BL/6 mice purchased from the National Cancer Institute. Tumors were allowed to develop for 2 to 3 weeks before harvesting for analysis. All mice were treated in accordance to procedures established by the UVA Animal Care and Use Committee protocol number 3292.

Human samples

Metastatic melanoma samples were collected with informed consent under UVA-IRB protocol number 10598. Excised tumors were processed by the UVA Biorepository and Tissue Procurement Facility Core using a protocol of an initial nonenzymatic disaggregation, followed by sequential incubations in a mixture of deoxyribonuclease/collagenase/hyaluronidase (*52*). Nondigested and digested fractions were stored in liquid nitrogen. Anonymous male and female healthy donor PBMCs were generated from Buffy coats purchased from Research Blood Components. PBMCs were isolated from the Buffy coat by density gradient centrifugation using Ficoll-Hypaque plus (VWR). PBMCs were cultured with interleukin-2 (IL-2; 10 IU/ml) alone or in combination with anti-CD3 (1 μg/ml; plate bound) and anti-CD28 (1 μg/ml; in solution), as indicated in the figure legends. The activity of enolase in the lysates of the human T_{eff} and TILs was assessed after FACS sorting the in vitro–stimulated healthy donor PBMCs and the ex vivo human melanoma TILs (nondigested tumor fractions) for live, $CD8^+$ or $CD4^+$ T cells that were $CD3^+CD45RO^+$ and $CD137^+$ or $CD137^-$. All sorts were performed under Biological Safety Level 2 (BSL-2) conditions using a Becton Dickinson Influx cell sorter by the UVA Flow Cytometry Core.

Checkpoint blockade treatment

Tumor-bearing mice received no treatment, intraperitoneal injection of 300 μg of control IgG (Equitech-Bio, Inc.), or a combination of 100 μg i.p. of each of anti–PD-1 (RMP1-14), anti–TIM-3 (RMP3-23) (both from H. Yagita, Juntendo University), and anti–CTLA-4 (9H10, BioXcell) with or without FTY-720 (2 μg/ml) on days 8, 11, and 14 after tumor injection. The FTY-720 treatment was continuously provided through the drinking water starting on day 8 after tumor injection. Tumor-bearing mice were treated with 250 μg of each of the antibodies in the monotherapy studies.

Adoptive T cell transfer

OT-1 T cells were in vitro stimulated with plate-bound anti-CD3 and soluble anti-CD28 (both at 5 μg/ml) and transferred (2 million cells per mouse intravenously) into day 5 B16cOVA tumor-bearing mice. Tumor size was measured every 3 days with a caliper. Mice were euthanized when tumor size reached 2000 mm^3.

T cell preparation, staining, and flow cytometric analysis

Splenocytes were isolated from the spleens of naive mice or mice that were immunized with a combination of 500 μg of OVA (Sigma-Aldrich), 75 μg of poly I:C (Invitrogen), and 100 μg of anti-CD40 (clone FGK45, provided by S. Schoenberger, La Jolla Institute) by mechanical homogenization followed by either density gradient separation with Lympholyte-M (Cedarlane) or RBC lysis (Affymetrix). For mouse TIL isolation, intact tumors were excised from mice and subjected to mechanical homogenization and density gradient separation as above. Samples were then stained with Live/Dead Aqua (Invitrogen), OVA_{257}-dextramer (Immudex), and a fluorescent conjugate antibody specific to surface proteins (CD8 and CD44). After surface staining, samples were fixed/permeabilized with 4% paraformaldehyde/0.1% Tween 20 in 1× phosphate-buffered saline (PBS) or cytofix/cytoperm (Becton Dickinson) and then stained with antibodies specific to intracellular proteins: p-PDK1 (Ser^{244}, Santa Cruz Biotechnology), p-mTORC1 (Ser^{2448}, Cell Signaling Technology), p-S6 (Ser^{235}/Ser^{236}, Cell Signaling Technology), p-4E-BP1 (Thr^{37}/Thr^{46}, Cell Signaling Technology), HIF1α (IC1935P, R&D Systems), PKM2 (D78A4, Cell Signaling Technology), GLUT1 (EPR3915, Abcam), ENOLASE 1 [EPR10863(B), Abcam], IFN-γ (XMG1.2, Thermo Fisher Scientific), TNFα (MP6-XT22, BioLegend), and secondary goat anti-rabbit FITC (ab6009, Abcam). FOXP3 fixation/permeabilization buffer and nuclear staining protocol (Thermo Fisher Scientific) were used to stain for HIF1α (241812, R&D Systems) and Ki67 (SolA15, Thermo Fisher Scientific).

T cells were in vitro stimulated with anti-CD3 (1 or 5 μg/ml; specified in figure legends) or OVA_{257} (10 μg/ml) peptide-pulsed, CD45-mismatched splenocytes for 4 hours before cytokine staining or for 1 hour before pS6 and p4E-BP1 staining. For PEP or pyruvate functional rescue experiments, cells were treated with dimethyl sulfoxide (vehicle), PEP (1 μg/ml; Sigma-Aldrich), or 1 mM pyruvate (Thermo Fisher Scientific) for 10 min on ice in glucose-free XF minimal media (Agilent). Saponin (0.005%; Sigma-Aldrich) was added to partially permeabilized cells to facilitate PEP entry, as previously described (*13*). Cells were then washed with 1× PBS and incubated at 37°C in a CO_2-free incubator in XF minimal media for 10 min to let the cells rest before proceeding to 4 hours of stimulation and cytokine staining. In the experiment involving analysis of cytokine production after acute inhibition of enolase activity, cells were in vitro stimulated with anti-CD3 (1 μg/ml) and IL-2 (10 IU/ml) for 24 hours in the presence of vehicle control (water) or 2 mM sodium fluoride (NaF). Brefeldin A was added only for the last 4 hours of the cell culture to enhance cytokine staining.

Flow cytometric analysis of the stained cells was conducted by using FACS Canto II (BD Scientific) or Cytoflex (Beckman Coulter) cytometers. Data were analyzed using FlowJo software (Version 10, TreeStar). To identify the T cell population of interest, we gated on live cells, lymphocytes, singlets, and $CD8^+$ cells followed by CD44lo and dextramer negative for naive T cells and CD44hi and dextramer positive for T_{eff} and TILs unless differently stated in the figure legend, as in the case of some in vitro restimulation experiments where total CD44hi T_{eff} and TILs were taken due to the impact of TCR stimulation on dextramer staining. For T cell sorting, single-cell suspensions of spleens or tumors were initially enriched for $CD8^+$ T cells by magnetic-activated cell sorting magnetic bead separation (Miltenyi Biotec) and then stained with OVA_{257} dextramer and antibody against surface antigens as above and placed in 4,6-diamidino-2-phenylindole (Sigma-Aldrich)–containing media sorted by using an Influx cell sorter (Becton Dickinson), applying stringent gating criterion to achieve >99% purity.

Glucose uptake

Splenocytes and TIL samples were prepared as described above and subjected to Live/Dead staining in 1× PBS at 4°C for 20 min followed by OVA_{257}-dextramer staining in 5% FBS at 4°C for 30 min. Cells were then incubated at 37°C and 5% CO_2 for 1 hour in glucose-free Dulbecco's modified Eagle's medium (DMEM) (Thermo Fisher Scientific) containing antibodies specific to surface proteins for cell identification. Cells were then washed with the glucose-free DMEM, further incubated under the above culture condition for 15 min in DMEM with or without 100 μM 2-NBDG (Thermo Fisher Scientific), and then washed in 1× PBS and immediately analyzed by flow cytometry while keeping samples on ice (*37*).

Analysis of enolase activity in in vitro and ex vivo T cell samples

Cell lysates were prepared according to the enolase activity kit protocol (Sigma-Aldrich) from FACS-sorted $CD8^+$ T cells and $CD8^+$ TILs directly ex vivo. Alternatively, T cells were cultured in vitro for 4 days with either IL-2 alone (10 IU/ml) or with plate-bound anti-CD3 (5 μg/ml), soluble anti-CD28 (2 μg/ml), and IL-2 (10 IU/ml). The lysates were then stored at −80°C until fluorometric direct enolase activity (PEP formation) assay was conducted according to the manufacturer's instructions. Fluorescence intensity was read at $\lambda_{ex} = 535/\lambda_{em} = 587$ nm for 45 to 60 min at 3-min intervals by using a Spectramax M5 plate reader (Molecular Devices) set to kinetic reading. In the experiments involving the inhibition of enolase activity, $CD8^+$ T cells from the spleens of the immunized mice were restimulated with plate-bound anti-CD3 (1 μg/ml), soluble anti-CD28 (2 μg/ml), and IL-2 (10 IU/ml) in the presence of 2 μM NaF or vehicle control (water). Alternatively, lysates prepared from in vitro $CD8^+$ T_{eff} generated as above were treated with 2 μM NaF or vehicle control for 5 min before reading enolase activity.

Metabolic assay

Naive $CD8^+$ T cells, T_{eff}, and $CD8^+$ TILs were FACS-sorted as described above, washed with 1× PBS, and seeded (2×10^5 cells per well) in an XFp cell culture miniplate in XF minimal media (Agilent) supplemented with 10 mM glucose (Sigma-Aldrich) and 2 mM glutamine (Invitrogen), with or without 2 mM sodium pyruvate (Thermo Fisher Scientific). ECAR and OCR were measured by extracellular flux analysis using XFp (Agilent) in response to 1 μM oligomycin, 1 μM FCCP, and 0.5 μM rotenone/antimycin (all from Sigma-Aldrich except antimycin, which was from MP Biochemicals). Radioactive-based measurement of glycolytic flux was performed through quantification of the amount of $[^3H]H_2O$ released from [3-^{3}H]glucose during glycolysis as described previously (*35*). Intracellular ATP levels of FACS-sorted naive $CD8^+$ T cells, T_{eff}, and $CD8^+$ TILs were determined by using the luciferase-based ATP Bioluminescence Assay Kit HS II (Cat# 11699709001, Roche). Cell lysates were prepared and processed for ATP measurement according to the assay kit protocol. The ATP-dependent light emitted during the luciferase reaction was measured by a luminometer (Zylux Femtomaster FB15, Zylux).

Metabolomics

FACS-sorted naive, effector, and tumor-infiltrating $CD8^+$ T cells were washed in RPMI plus 10% FBS, resuspended in prechilled 80% methanol/water on dry ice, and transferred to a −80°C freezer for 15 min to disrupted cell membrane and quench enzymatic activities. Samples were then vortexed while being kept cold and spun down at 16,000 relative centrifugal force in a tabletop centrifuge to extract the metabolites. Supernatants were harvested and dried by SpeedVac. Samples were then processed and subjected to liquid chromatography–mass spectrometry analysis as previously described (*40*).

RNA extraction, cDNA synthesis, and real-time qPCR

Total RNA was extracted from FACS-sorted naive $CD8^+$ T cells, T_{eff}, and $CD8^+$ TILs with the RNeasy Plus Kit (Qiagen) and then reverse-transcribed into complementary DNA (cDNA) using the iScript cDNA Synthesis Kit (Bio-Rad). SYBR Green–based real-time qPCR analysis was performed using the CFX96 Detection System (Bio-Rad). All samples were run in biological triplicates and normalized to ribosomal protein S18 (Rps18). Fold change in gene expression level was determined by the $\Delta\Delta C_t$ method comparing the expression level of each sample to that of naive $CD8^+$ T cells. The sequences of the primers are as follows:

Gene	Forward primers	Reverse primers
RPS18S	5′-ATGCGGC GGCGTTATTCC-3′	5′-GCTATCAATCGTT-CAATCCTGTCC-3′
GLUT1	5′-CAGTTCGGCTAT-AACACTGGTG-3′	5′-GCCCCCGAC-AGAGAAGATG-3′
mGlut3	5′-TAAACCAGCTGG-GCATCGTTGTTG-3′	5′-AATGATGGTTAAG-CCAAGGAGCCC-3′
Hk2	5′-TGATCGCCTGCTT-ATTCACGG-3′	5′-AACCGCCTAGA-AATCTCCAGA-3′
Pfkm	5′-GGAAAGGAAGACA-GAGTGGGAGGC-3′	5′-CAGATCGACCTCAA-CAGTGGGATTC-3′
Pfkp	5′-GGTACAGATTC-AGCCCTGCACC-3′	5′-GTCGGCACCG-CAAGTCAAGG-3′
GAPDH	5′-GTCGGTGTGA-ACGGATTTG-3′	5′-TAGACTCCACGA-CATACTCAGCA-3′
Pgm3	5′-CCCAGCATCTCGAT-CATATCATGTTTCG-3′	5′-GTCCTGCTCC-TCCGCACTGG-3′
Eno1	5′-GGAAAGGAAGAC-AGAGTGGGAGGC-3′	5′-CAGATCGACCTCA-ACAGTGGGATTC-3′
Ldha	5′-CATTGTCAAGTAC-AGTCCACACT-3′	5′-TTCCAATTACTC-GGTTTTTGGGA-3′
Ldhb	5′-GGACAAGTGGG-TATGGCATGTG-3′	5′-CCGTCACCACC-ACAATCTTAGA-3′
MCT4	5′-TCACGGGTTT-CTCCTACGC-3′	5′-GCCAAAGCG-GTTCACACAC-3′

Statistical analysis

All data are presented as means ± SEM. Statistical significance was determined by unpaired Student's *t* test when comparing two groups and by one-way analysis of variance (ANOVA) or two-way ANOVA, followed by Tukey's multiple comparison test when comparing more than two groups. GraphPad Prism 7 was used to perform the statistics.

SUPPLEMENTARY MATERIALS

immunology.sciencemag.org/cgi/content/full/4/31/eaap9520/DC1

Fig. S1. B16cOVA-infiltrating CD8$^+$ TILs exhibit phenotypic and functional markers of exhaustion.

Fig. S2. CD8$^+$ TILs express high levels of glucose transporters.

Fig. S3. The abundance of glycolytic enzymes and metabolites suggests that PEP deficiency of CD8$^+$ TILs is driven by lack of strong enolase activity.

Fig. S4. Inhibition of the enolase activity in T cells limits cytokine production.

Fig. S5. Enolase activity contributes to the effector function of CPi-treated CD8$^+$ TILs.

Fig. S6. Human melanoma TILs have low function and enolase activity.

Table S1. Raw data file.

REFERENCES AND NOTES

1. C. G. Clemente, M. C. Mihm Jr., R. Bufalino, S. Zurrida, P. Collini, N. Cascinelli, Prognostic value of tumor infiltrating lymphocytes in the vertical growth phase of primary cutaneous melanoma. *Cancer* **77**, 1303–1310 (1996).
2. L. Zhang, J. R. Conejo-Garcia, D. Katsaros, P. A. Gimotty, M. Massobrio, G. Regnani, A. Makrigiannakis, H. Gray, K. Schlienger, M. N. Liebman, S. C. Rubin, G. Coukos, *Intratumoral T Cells, Recurrence, and Survival in Epithelial Ovarian Cancer* (Massachusetts Medical Society, 2003), pp. 203–213.
3. J. Galon, A. Costes, F. Sanchez-Cabo, A. Kirilovsky, B. Mlecnik, C. Lagorce-Pagès, M. Tosolini, M. Camus, A. Berger, P. Wind, F. Zinzindohoué, P. Bruneval, P.-H. Cugnenc, Z. Trajanoski, W.-H. Fridman, F. Pagès, Type, density, and location of immune cells within human colorectal tumors predict clinical outcome. *Science* **313**, 1960–1964 (2006).
4. J. Crespo, H. Sun, T. H. Welling, Z. Tian, W. Zou, T cell anergy, exhaustion, senescence and stemness in the tumor microenvironment. *Curr. Opin. Immunol.* **25**, 214–221 (2013).
5. M. Ahmadzadeh, L. A. Johnson, B. Heemskerk, J. R. Wunderlich, M. E. Dudley, D. E. White, S. A. Rosenberg, Tumor antigen-specific CD8 T cells infiltrating the tumor express high levels of PD-1 and are functionally impaired. *Blood* **114**, 1537–1544 (2009).
6. D. M. Pardoll, The blockade of immune checkpoints in cancer immunotherapy. *Nat. Rev. Cancer* **12**, 252–264 (2012).
7. J. Duraiswamy, G. Freeman, G. Coukos, Replenish the source within: Rescuing tumor-infiltrating lymphocytes by double checkpoint blockade. *Oncoimmunology* **2**, e25912 (2013).
8. M. Singer, C. Wang, L. Cong, N. D. Marjanovic, M. S. Kowalczyk, H. Zhang, J. Nyman, K. Sakuishi, S. Kurtulus, D. Gennert, J. Xia, J. Y. H. Kwon, J. Nevin, R. H. Herbst, I. Yanai, O. Rozenblatt-Rosen, V. K. Kuchroo, A. Regev, A. C. Anderson, A distinct gene module for dysfunction uncoupled from activation in tumor-infiltrating T cells. *Cell* **171**, 1221–1223 (2017).
9. N. Chihara, A. Madi, T. Kondo, H. Zhang, N. Acharya, M. Singer, J. Nyman, N. D. Marjanovic, M. S. Kowalczyk, C. Wang, S. Kurtulus, T. Law, Y. Etminan, J. Nevin, C. D. Buckley, P. R. Burkett, J. D. Buenrostro, O. Rozenblatt-Rosen, A. C. Anderson, A. Regev, V. K. Kuchroo, Induction and transcriptional regulation of the co-inhibitory gene module in T cells. *Nature* **558**, 454–459 (2018).
10. K. E. Pauken, E. J. Wherry, Overcoming T cell exhaustion in infection and cancer. *Trends Immunol.* **36**, 265–276 (2015).
11. C.-H. Chang, J. Qiu, D. O'Sullivan, M. D. Buck, T. Noguchi, J. D. Curtis, Q. Chen, M. Gindin, M. M. Gubin, G. J. W. van der Windt, E. Tonc, R. D. Schreiber, E. J. Pearce, E. L. Pearce, Metabolic competition in the tumor microenvironment is a driver of cancer progression. *Cell* **162**, 1229–1241 (2015).
12. N. E. Scharping, A. V. Menk, R. S. Moreci, R. D. Whetstone, R. E. Dadey, S. C. Watkins, R. L. Ferris, G. M. Delgoffe, The tumor microenvironment represses T cell mitochondrial biogenesis to drive intratumoral T cell metabolic insufficiency and dysfunction. *Immunity* **45**, 374–388 (2016).
13. P.-C. Ho, J. D. Bihuniak, A. N. Macintyre, M. Staron, X. Liu, R. Amezquita, Y.-C. Tsui, G. Cui, G. Micevic, J. C. Perales, S. H. Kleinstein, E. D. Abel, K. L. Insogna, S. Feske, J. W. Locasale, M. W. Bosenberg, J. C. Rathmell, S. M. Kaech, Phosphoenolpyruvate is a metabolic checkpoint of anti-tumor T cell responses. *Cell* **162**, 1217–1228 (2015).
14. N. E. Scharping, A. V. Menk, R. D. Whetstone, X. Zeng, G. M. Delgoffe, Efficacy of PD-1 blockade is potentiated by metformin-induced reduction of tumor hypoxia. *Cancer Immunol. Res.* **5**, 9–16 (2017).
15. C. M. Cham, G. Driessens, J. P. O'Keefe, T. F. Gajewski, Glucose deprivation inhibits multiple key gene expression events and effector functions in CD8$^+$ T cells. *Eur. J. Immunol.* **38**, 2438–2450 (2008).
16. E. L. Pearce, M. C. Poffenberger, C.-H. Chang, R. G. Jones, Fueling immunity: Insights into metabolism and lymphocyte function. *Science* **342**, 1242454 (2013).
17. C.-H. Chang, J. D. Curtis, L. B. Maggi Jr., B. Faubert, A. V. Villarino, D. O'Sullivan, S. C.-C. Huang, G. J. W. van der Windt, J. Blagih, J. Qiu, J. D. Weber, E. J. Pearce, R. G. Jones, E. L. Pearce, Posttranscriptional control of T cell effector function by aerobic glycolysis. *Cell* **153**, 1239–1251 (2013).
18. R. Wang, C. P. Dillon, L. Z. Shi, S. Milasta, R. Carter, D. Finkelstein, L. L. McCormick, P. Fitzgerald, H. Chi, J. Munger, D. R. Green, The transcription factor Myc controls metabolic reprogramming upon T lymphocyte activation. *Immunity* **35**, 871–882 (2011).
19. C. E. Widjaja, J. G. Olvera, P. J. Metz, A. T. Phan, J. N. Savas, G. de Bruin, Y. Leestemaker, C. R. Berkers, A. de Jong, B. I. Florea, K. Fisch, J. Lopez, S. H. Kim, D. A. Garcia, S. Searles, J. D. Bui, A. N. Chang, J. R. Yates III, A. W. Goldrath, H. S. Overkleeft, H. Ovaa, J. T. Chang, Proteasome activity regulates CD8$^+$ T lymphocyte metabolism and fate specification. *J. Clin. Invest.* **127**, 3609–3623 (2017).
20. D. K. Finlay, E. Rosenzweig, L. V. Sinclair, C. Feijoo-Carnero, J. L. Hukelmann, J. Rolf, A. A. Panteleyev, K. Okkenhaug, D. A. Cantrell, PDK1 regulation of mTOR and hypoxia-inducible factor 1 integrate metabolism and migration of CD8$^+$ T cells. *J. Exp. Med.* **209**, 2441–2453 (2012).
21. A. N. Macintyre, D. Finlay, G. Preston, L. V. Sinclair, C. M. Waugh, P. Tamas, C. Feijoo, K. Okkenhaug, D. A. Cantrell, Protein kinase B controls transcriptional programs that direct cytotoxic T cell fate but is dispensable for T cell metabolism. *Immunity* **34**, 224–236 (2011).
22. S. R. Jacobs, C. E. Herman, N. J. Maciver, J. A. Wofford, H. L. Wieman, J. J. Hammen, J. C. Rathmell, Glucose uptake is limiting in T cell activation and requires CD28-mediated Akt-dependent and independent pathways. *J. Immunol.* **180**, 4476–4486 (2008).
23. D. K. Finlay, Regulation of glucose metabolism in T cells: New insight into the role of Phosphoinositide 3-kinases. *Front. Immunol.* **3**, 247 (2012).
24. A. T. Waickman, J. D. Powell, mTOR, metabolism, and the regulation of T-cell differentiation and function. *Immunol. Rev.* **249**, 43–58 (2012).

25. C. M. Cham, T. F. Gajewski, Glucose availability regulates IFN-γ production and p70S6 kinase activation in CD8$^+$ effector T cells. *J. Immunol.* **174**, 4670–4677 (2005).
26. Y. Cao, J. C. Rathmell, A. N. Macintyre, Metabolic reprogramming towards aerobic glycolysis correlates with greater proliferative ability and resistance to metabolic inhibition in CD8 versus CD4 T cells. *PLOS ONE* **9**, e104104 (2014).
27. M. G. Vander Heiden, L. C. Cantley, C. B. Thompson, Understanding the Warburg effect: The metabolic requirements of cell proliferation. *Science* **324**, 1029–1033 (2009).
28. S. Y. Lunt, M. G. Vander Heiden, Aerobic glycolysis: Meeting the metabolic requirements of cell proliferation. *Annu. Rev. Cell Dev. Biol.* **27**, 441–464 (2011).
29. N. J. MacIver, R. D. Michalek, J. C. Rathmell, Metabolic regulation of T lymphocytes. *Annu. Rev. Immunol.* **31**, 259–283 (2013).
30. Y. Zheng, G. M. Delgoffe, C. F. Meyer, W. Chan, J. D. Powell, Anergic T cells are metabolically anergic. *J. Immunol.* **183**, 6095–6101 (2009).
31. B. Bengsch, A. L. Johnson, M. Kurachi, P. M. Odorizzi, K. E. Pauken, J. Attanasio, E. Stelekati, L. M. McLane, M. A. Paley, G. M. Delgoffe, E. J. Wherry, Bioenergetic insufficiencies due to metabolic alterations regulated by the inhibitory receptor PD-1 are an early driver of CD8$^+$ T cell exhaustion. *Immunity* **45**, 358–373 (2016).
32. P. J. Siska, K. E. Beckermann, F. M. Mason, G. Andrejeva, A. R. Greenplate, A. B. Sendor, Y.-C. J. Chiang, A. L. Corona, L. F. Gemta, B. G. Vincent, R. C. Wang, B. Kim, J. Hong, C.-I. Chen, T. N. Bullock, J. M. Irish, W. K. Rathmell, J. C. Rathmell, Mitochondrial dysregulation and glycolytic insufficiency functionally impair CD8 T cells infiltrating human renal cell carcinoma. *JCI Insight* **2**, e93411 (2017).
33. D. J. Roberts, N. A. Franklin, L. M. Kingeter, H. Yagita, A. L. Tutt, M. J. Glennie, T. N. J. Bullock, Control of established melanoma by CD27 stimulation is associated with enhanced effector function and persistence, and reduced PD-1 expression, of tumor infiltrating CD8$^+$T cells. *J. Immunother.* **33**, 769–779 (2010).
34. R. D. Michalek, J. C. Rathmell, The metabolic life and times of a T-cell. *Immunol. Rev.* **236**, 190–202 (2010).
35. F. L. Byrne, I. K. H. Poon, S. C. Modesitt, J. L. Tomsig, J. D. Y. Chow, M. E. Healy, W. D. Baker, K. A. Atkins, J. M. Lancaster, D. C. Marchion, K. H. Moley, K. S. Ravichandran, J. K. Slack-Davis, K. L. Hoehn, Metabolic vulnerabilities in endometrial cancer. *Cancer Res.* **74**, 5832–5845 (2014).
36. A. N. Macintyre, V. A. Gerriets, A. G. Nichols, R. D. Michalek, M. C. Rudolph, D. Deoliveira, S. M. Anderson, E. D. Abel, B. J. Chen, L. P. Hale, J. C. Rathmell, The glucose transporter GLUT1 is selectively essential for CD4 T cell activation and effector function. *Cell Metab.* **20**, 61–72 (2014).
37. S. Sengupta, R. J. Vitale, P. M. Chilton, T. C. Mitchell, in *Advances in Experimental Medicine and Biology* (Springer US, 2008), vol. 614, pp. 65–72.
38. D. K. Finlay, mTORC1 regulates CD8$^+$ T-cell glucose metabolism and function independently of PI3K and PKB. *Biochem. Soc. Trans.* **41**, 681–686 (2013).
39. E. L. Pearce, E. J. Pearce, Metabolic pathways in immune cell activation and quiescence. *Immunity* **38**, 633–643 (2013).
40. X. Liu, Z. Ser, J. W. Locasale, Development and quantitative evaluation of a high-resolution metabolomics technology. *Anal. Chem.* **86**, 2175–2184 (2014).
41. H. Cho, J. Um, J.-H. Lee, W.-H. Kim, W. S. Kang, S. H. Kim, H.-H. Ha, Y.-C. Kim, Y.-K. Ahn, D.-W. Jung, D. R. Williams, ENOblock, a unique small molecule inhibitor of the non-glycolytic functions of enolase, alleviates the symptoms of type 2 diabetes. *Sci. Rep.* **7**, 44186 (2017).
42. D.-W. Jung, W.-H. Kim, S.-H. Park, J. Lee, J. Kim, D. Su, H.-H. Ha, Y.-T. Chang, D. R. Williams, A unique small molecule inhibitor of enolase clarifies its role in fundamental biological processes. *ACS Chem. Biol.* **8**, 1271–1282 (2013).
43. N. Patsoukis, K. Bardhan, P. Chatterjee, D. Sari, B. Liu, L. N. Bell, E. D. Karoly, G. J. Freeman, V. Petkova, P. Seth, L. Li, V. A. Boussiotis, PD-1 alters T-cell metabolic reprogramming by inhibiting glycolysis and promoting lipolysis and fatty acid oxidation. *Nat. Commun.* **6**, 6692 (2015).
44. Y. Zhu, L. Chen, CD137 as a biomarker for tumor-reactive T cells: Finding gold in the desert. *Clin. Cancer Res.* **20**, 3–5 (2014).
45. W. C. Hallows, W. Yu, J. M. Denu, Regulation of glycolytic enzyme phosphoglycerate mutase-1 by Sirt1 protein-mediated deacetylation. *J. Biol. Chem.* **287**, 3850–3858 (2012).
46. T. Hitosugi, L. Zhou, S. Elf, J. Fan, H.-B. Kang, J. H. Seo, C. Shan, Q. Dai, L. Zhang, J. Xie, T.-L. Gu, P. Jin, M. Alečković, G. LeRoy, Y. Kang, J. A. Sudderth, R. J. DeBerardinis, C.-H. Luan, G. Z. Chen, S. Muller, D. M. Shin, T. K. Owonikoko, S. Lonial, M. L. Arellano, H. J. Khoury, F. R. Khuri, B. H. Lee, K. Ye, T. J. Boggon, S. Kang, C. He, J. Chen, Phosphoglycerate mutase 1 coordinates glycolysis and biosynthesis to promote tumor growth. *Cancer Cell* **22**, 585–600 (2012).
47. W. Zhou, M. Capello, C. Fredolini, L. Piemonti, L. A. Liotta, F. Novelli, E. F. Petricoin, Mass spectrometry analysis of the post-translational modifications of α-enolase from pancreatic ductal adenocarcinoma cells. *J. Proteome Res.* **9**, 2929–2936 (2010).
48. H. Ji, J. Wang, J. Guo, Y. Li, S. Lian, W. Guo, H. Yang, F. Kong, L. Zhen, L. Guo, Y. Liu, Progress in the biological function of α-enolase. *Anim. Nutr.* **2**, 12–17 (2016).
49. S. Gao, H. L. Li, Y. Cai, J. Ye, Z.-P. Liu, J. H. Lu, X.-Y. Huang, X.-j. Feng, H. Gao, S.-r. Chen, M. Li, P. Liu, Mitochondrial binding of α-enolase stabilizes mitochondrial membrane: Its role in doxorubicin-induced cardiomyocyte apoptosis. *Arch. Biochem. Biophys.* **542**, 46–55 (2014).
50. K. C. Sedoris, S. D. Thomas, D. M. Miller, C-Myc promoter binding protein regulates the cellular response to an altered glucose concentration. *Biochemistry* **46**, 8659–8668 (2007).
51. M. L. Hwang, J. R. Lukens, T. N. J. Bullock, Cognate memory CD4$^+$ T cells generated with dendritic cell priming influence the expansion, trafficking, and differentiation of secondary CD8$^+$ T cells and enhance tumor control. *J. Immunol.* **179**, 5829–5838 (2007).
52. E. P. Salerno, W. C. Olson, C. McSkimming, S. Shea, C. L. Slingluff Jr., T cells in the human metastatic melanoma microenvironment express site-specific homing receptors and retention integrins. *Int. J. Cancer* **134**, 563–574 (2014).

Acknowledgments: We thank S. Jeong for technical support with human sample processing and D. Kashatus for critical review of the manuscript. **Funding:** This study was supported by NIH grant R01CA166458-03S1 (CRCHD Diversity Supplements to L.F.G.), a UVA Immunology Training Grant (5T32AI007496-19 to L.F.G.), grant R01CA166458 (to T.N.J.B), and grants R01DK105550 and R01CA217987 (both to J.C.R.). **Author contributions:** L.F.G. designed and performed experiments, analyzed the data, and wrote the manuscript. P.J.S. and J.C.R. designed and performed some of the experiments. M.E.N., X.G., X.L., J.W.L., and K.L.H. acquired and analyzed some of the data. H.Y. and C.L.S. provided reagents/samples. T.N.J.B. supervised all the studies and contributed to writing the manuscript. All coauthors reviewed the manuscript. **Competing interests:** The authors declare that they have no competing interests. **Data and materials availability:** The metabolomics data for this study have been deposited in Mendeley Data: T. Bullock, J. Locasale, L. Gemta (2018), "Metabolomic analysis of CD8$^+$ naive, effector and TILs", Mendeley Data, v1 (http://dx.doi.org/10.17632/wmrwjdbg82.1).

Submitted 13 September 2017
Resubmitted 10 August 2018
Accepted 3 December 2018
Published 25 January 2019
10.1126/sciimmunol.aap9520

Citation: L. F. Gemta, P. J. Siska, M. E. Nelson, X. Gao, X. Liu, J. W. Locasale, H. Yagita, C. L. Slingluff Jr., K. L. Hoehn, J. C. Rathmell, T. N. J. Bullock, Impaired enolase 1 glycolytic activity restrains effector functions of tumor-infiltrating CD8$^+$ T cells. *Sci. Immunol.* **4**, eaap9520 (2019).

Science Immunology

Impaired enolase 1 glycolytic activity restrains effector functions of tumor-infiltrating CD8$^+$ T cells

Lelisa F. Gemta, Peter J. Siska, Marin E. Nelson, Xia Gao, Xiaojing Liu, Jason W. Locasale, Hideo Yagita, Craig L. Slingluff, Jr., Kyle L. Hoehn, Jeffrey C. Rathmell and Timothy N. J. Bullock

Sci. Immunol. **4**, eaap9520.
DOI: 10.1126/sciimmunol.aap9520

Rescuing T cell glycolysis

One reason T cells in the tumor microenvironment (TME) become dysfunctional is that they compete with cancer cells for nutrients, particularly glucose. By studying the glucose metabolism of CD8$^+$ T cells in the TME of mouse B16 and human melanomas, Gemta *et al*. report the activity of enzyme enolase 1 to be impaired. Enolase 1 catalyzes the synthesis of phosphenolpyruvate, which is dephosphorylated to generate pyruvate, the end product of glycolysis. In vitro, provision of pyruvate considerably improved the effector functions of CD8$^+$ T cells isolated from murine melanomas. Pinning down enolase 1 as the rate-limiting step in glucose metabolism of tumor-infiltrating T cells begs the question whether targeting enolase 1 activity in these cells can be used to improve responsiveness to cancer immunotherapy.